Proc. of the European Safety and Reliability Conference (ESREL 2026)
Edited by José C. Matos, Paulo B. Lourenço, Michael Beer, Daniel Oliveira, Edoardo Patelli, Hélder S. Sousa, Rui A. Silva and Monica Santamaria

doi: 10.3850/ESREL2026061419_esrel26-p26349-cd

Numerical Study of Hydrogen Dispersion in A Stationary Ni-Cd Battery Room Under Multiple Leak Conditions

Muchen Zhang

Centre for Technological Risk Studies (CERTEC), Universitat Politècnica de Catalunya, Spain.
E-mail: muchen.zhang@upc.edu

Miguel Muñoz Messineo

Process Safety and Major Accidents Department, NOVOTEC, Spain. E-mail: miguel.munoz.m@novotec.es

David Bartumeus Vallespí

Process Safety and Major Accidents Department, NOVOTEC, Spain. E-mail: david.bartumeus@applus.com

Pascale Vacca

Centre for Technological Risk Studies (CERTEC), Universitat Politècnica de Catalunya, Spain.
E-mail: pascale.vacca@upc.edu

Eulàlia Planas

Centre for Technological Risk Studies (CERTEC), Universitat Politècnica de Catalunya, Spain.
E-mail: eulalia.planas@upc.edu

The charging of nickel–cadmium (Ni-Cd) batteries in enclosed environments can lead to hydrogen accumulation, posing explosion hazards if ventilation is inadequate. This study applies computational fluid dynamics (CFD) to analyze hydrogen dispersion from stationary vented Ni-Cd batteries under different leak scenarios. The objective is to understand hydrogen accumulation behavior and verify compliance with safety requirements such as the ATEX Directive 2014/34/EU. The analyzed scenario includes a full-scale battery storage room containing typical Ni-Cd installations, simulations were conducted using FLACS, accounting for buoyancy-driven transport, turbulent dispersion, and realistic vent geometries. The study investigates three charging modes (float, boost and exceptional), each corresponding to different hydrogen generation rates. Two ventilation modes are examined to assess their influence on hydrogen accumulation and dispersion. Furthermore, the study discusses whether the simplified ventilation calculation method defined in the regulations provides sufficient safety margins for these operating conditions. The results highlight that hydrogen dispersion is strongly affected by both the release characteristics and the ventilation configuration, demonstrating the need for a detailed assessment of ventilation performance beyond simplified standard calculations. This work demonstrates the capability of CFD to support quantitative safety evaluation of Ni-Cd battery installations. The modeling approach provides a practical framework for verifying ventilation performance and assessing the conservativeness of standard-based design methods. The outcomes contribute to improved design and risk management for stationary battery systems in enclosed environments.

Keywords: Hydrogen dispersion, Ni-Cd battery, ventilation, CFD, FLACS.

1. Introduction

Nickel-cadmium (Ni-Cd) battery systems, widely used for backup power in industrial and grid applications, can release hydrogen gas during charging. In an enclosed room, the generated hydrogen can accumulate near the ceiling due to buoyancy and form a flammable mixture if not adequately ventilated. Hydrogen has a wide flammability range (about 4–75% by volume in air) and an extremely low ignition energy (around 0.017 mJ) (Nan et al., 2024). These hazards underscore the importance of managing hydrogen emissions in Ni–Cd battery installations to prevent the formation of explosive atmospheres.

Recognizing this hazard, safety standards and regulations provide guidelines for battery room design and classification. In the European Union, the ATEX Directive (2014/34/EU) and related standards (e.g. IEC 60079-10-1) require classification of areas with potential explosive atmospheres (European Parliament and the Council, 2014; International Electrotechnical Commission, 2022). In particular, the 25% of the LFL (Lower Flammability Limit) value is the safety margin required for monitoring and control systems in these environments to trigger alarms or initiate emergency ventilation (International Electrotechnical Commission, 2022). Ventilation requirements for stationary battery installations are also outlined in standards such as IEC 62485-2 (International Electrotechnical Commission, 2010), where simplified calculations are prescribed to ensure a safe dilution of hydrogen inside the facility. However, these methods do not account for spatial variations in gas concentration, nor the effects of room geometry and ventilation layout. In addition, hydrogen generation from batteries is often treated as a single equivalent point source, which is another aspect that is not explicitly considered in standards such as IEC 60079-10-2. In reality, hydrogen is released from distributed vent openings or multiple small locations across the battery surfaces, it will stratify towards the ceiling and may form localized pockets of higher concentration if ventilation is not well-distributed. Similar source simplifications are also adopted in some CFD (Computational Fluid Dynamics) studies (Brzezińska, 2018), which may limit their ability to capture realistic dispersion patterns in enclosed battery rooms.

Given these shortcomings, CFD has been proven to be a powerful tool in modeling these phenomena. A full-scale study combining experiments and CFD simulations was conducted by Brzezińska (2018), it was found that low hydrogen emission rates can lead to uniform accumulation reaching the LEL (Lower Explosive Limit) throughout the room, concluding that effective ventilation is essential to mitigate explosion risk. Similarly, ElNakeeb et al. (2017) also used a CFD tool to study a Ni–Cd battery storage room, finding that optimizing the placement of inlet and outlet vents can keep hydrogen concentrations within safe limits. Such computational studies provide valuable insights for layout optimization, hazard assessments and mitigation strategy selection in battery installations.

To conclude, most of the existing work primarily focuses on evaluating the effects of ventilation layout or room geometry. There is a lack of detailed analysis on whether hydrogen pockets may form under real-world charging conditions, even when simplified ventilation criteria from standards are met. In this study, we use the FLACS CFD tool to model hydrogen dispersion from Ni-Cd battery systems under three charging scenarios (float, boost, and exceptional) in a full-scale battery room, considering both natural and forced ventilation. The aim of the current study is to evaluate the risk of hydrogen accumulation inside the room and assess whether standard-based ventilation design offers sufficient safety margins. In this paper, the methodology of developing this numerical model is elaborated in Section 2, including the numerical setups and description of case studies; the results and discussion of the case studies are shown in Section 3; and finally, the conclusions are drawn in Section 4.

2. Methodology

2.1. *Numerical setups*

The hydrogen dispersion is simulated with the commercial CFD code FLACS (version 24.2), which solves the three–dimensional, transient, compressible Reynolds–averaged Navier–Stokes equations with a k–ε turbulence model and species transport for hydrogen–air mixtures. Hydrogen is treated as an ideal gas with full buoyancy effects, and density variations are captured through the equation of state (Gexcon AS, 2025).

2.1.1. *Geometric configuration*

The case represents a full–scale Ni–Cd battery room in a real-life plant. The inner room has dimensions $L_{\text{in}} \times W_{\text{in}} \times H_{\text{in}} = 8.44 \times 6.29 \times 7.40\ \text{m}^3$, while the computational domain extends to $11.0 \times 9.0 \times 9.0\ \text{m}^3$ to include buffer zones around the room (Lu and Gong, 2021). Inside the room, four parallel benches are aligned as shown in Figure 1 and host four groups of vented Ni–Cd monoblocks: two groups of 92 cells (440 Ah) and two groups of 38 cells (250 Ah).

Hydrogen generation from the monoblocks is represented by rectangular area sources on the top surface of each bench. As shown in Figure 2, two ventilation outlets with sizes of 0.45×0.45 m^2 are located near the ceiling on wall $Y0$ and are modeled as *Suction* leaks in FLACS. In addition, five lower openings (four on wall $Y0$ and one on wall $Y1$) act as natural inlets/outlets, allowing air to enter or leave depending on the pressure field. The geometry and vent layout are consistent across all simulations, only the ventilation profiles and hydrogen generation rates are varied between cases.

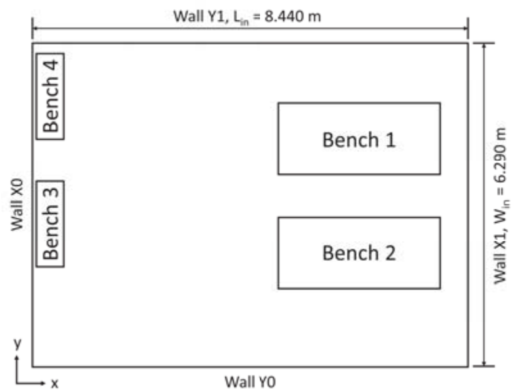

Fig. 1. Battery room layout in x-y plane.

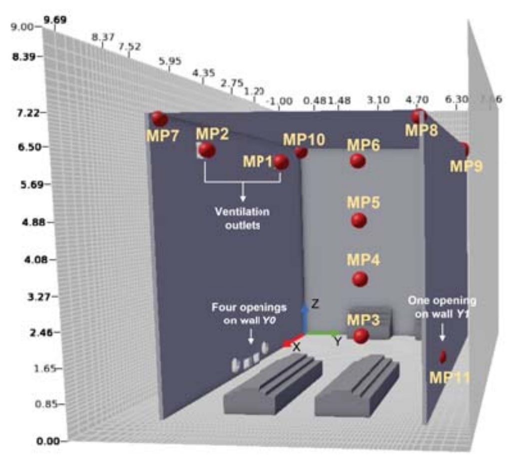

Fig. 2. 3D geometry of the battery room and the locations of the monitors (wall *X1* is hidden).

2.1.2. *Boundary and initial conditions*

All simulations are conducted as transient calculations. At the beginning of each case, there is no wind inside the room, with an initial temperature of $20°$C and an ambient pressure of 1 bar. The computational domain is initially filled with air containing no hydrogen. The floor is treated as a solid boundary (*Euler* type in FLACS), while all other outer boundaries are defined as open boundaries (*Nozzle* type in FLACS), allowing gas to flow into or out of the domain according to the local pressure conditions (Lu and Gong, 2021).

Hydrogen release from the battery monoblocks is modeled using the *Area Leak* concept in FLACS. The hydrogen sources are defined as *Diffuse* area leaks with a uniform release profile, distributed over the bench-top surfaces. The release direction is set vertically upward $(+Z)$, representing buoyancy-driven hydrogen emission from vented battery cells during charging without imposing artificial jet momentum.

Both natural and forced ventilation scenarios are considered. In all cases, the same two ventilation openings located near the ceiling on wall *Y0* are used as outlets and are modeled as *Suction*-type area leaks, with the leak direction pointing outward from the room. According to the FLACS user manual (Gexcon AS, 2025), a suction leak acts as a mass sink and removes all fluid passing through the outlet, with the extracted mixture composition determined by the local flow field rather than being prescribed. This approach enables a physically consistent representation of hydrogen removal by ventilation.

Time-step control follows the FLACS recommendations for dispersion and ventilation simulations, using a Courant number based on the speed of sound of $\text{CFLC} = 10$ and a velocity-based Courant number of $\text{CFLV} = 1$.

2.1.3. *Grid Independence Analysis*

The FLACS solver uses a structured Cartesian mesh. A grid independence analysis was conducted using three sets of systematically refined grids (coarse, medium, and fine), as summarized in Table 1. The three grids share the same block structure and geometric discretizations, with refinement applied primarily near the battery benches and ventilation openings in upper part of the room. The characteristic cell size in the core region is reduced by approximately a factor of two between successive grid levels, following mesh refinement practices commonly adopted in grid convergence and GCI (Grid Convergence Index)-based studies (Roache, 1997; American Society of Mechanical Engineers (ASME), 2008).

Table 1. Summary of the three grid levels used for the grid independence analysis.

Grid level	Total cells	Core Δx (m)	Core Δy (m)	Core Δz (m)
Fine	3,269,505	≈ 0.05	≈ 0.05–0.06	≈ 0.05
Medium	559,872	≈ 0.10	≈ 0.10	≈ 0.10
Coarse	114,400	≈ 0.17–0.20	≈ 0.20–0.22	≈ 0.18

Grid independence was evaluated by comparing the transient evolution of hydrogen concentration at a representative monitoring location at the ventilation outlet under exceptional charging conditions. Figure 3 shows the comparison among the three grids. The coarse grid predicts significantly lower hydrogen concentrations and exhibits delayed plume development, indicating insufficient resolution. In contrast, the medium and fine grids show similar temporal trends and magnitudes after the initial transient phase, with only minor differences observed at later times. Based on this comparison, the medium grid is considered adequate for capturing the hydrogen dispersion behavior with acceptable accuracy and computational efficiency.

2.2. *Case Studies*

To investigate hydrogen dispersion under representative operating conditions, a set of case studies was defined by combining different ventilation modes and battery charging scenarios. The selected cases are summarized in Table 2 and include natural ventilation under float charging, as well as forced ventilation under boost and exceptional charging modes. The three charging modes represent progressively higher operating currents and associated hydrogen generation rates: float corresponds to maintenance (trickle) charging, boost to an elevated recharge mode, and exceptional to a high-rate (worst-case) charging condition. The detailed per–cell generation rates are calculated from IEC 62485–2 and then converted to equivalent area leaks on each bench (International Electrotechnical Commission, 2010). For each mode, the total hydrogen mass release rate $\dot{m}_{\mathrm{H}_2}$ is also shown in Table 2, it is obtained from the per-cell generation rates and the number of cells on each bench, and is uniformly distributed over the corresponding bench leak areas.

The ventilation settings are based on the actual site conditions. For natural ventilation, an air change rate of $\mathrm{ACH_n} = 1\ \mathrm{h}^{-1}$ is assumed. For forced ventilation, a fan capacity of $Q_\mathrm{f} = 7{,}540\ \mathrm{m}^3/\mathrm{h}$ is imposed, equals to $\mathrm{ACH_f} \approx 19\ \mathrm{h}^{-1}$. Based on an effective room volume of $395.45\ \mathrm{m}^3$, the corresponding mass flow rates per ventilation opening are calculated as $\dot{m}_\mathrm{n} = 0.0673\ \mathrm{kg/s}$ for natural ventilation and $\dot{m}_\mathrm{f} = 1.2828\ \mathrm{kg/s}$ for forced ventilation, assuming the extracted gas at the ventilation outlets to be air for the purpose of mass flow rate calculation.

In all cases, hydrogen release is activated after an initial period in which ventilation is allowed to establish a stable flow field. Specifically, hydrogen

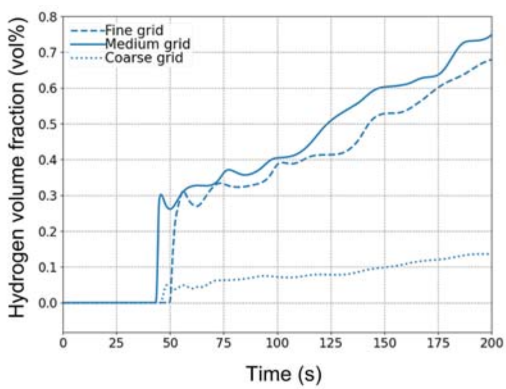

Fig. 3. Grid independence analysis using hydrogen volume fraction (vol%) at one of the ventilation outlets.

generation starts at $t = 200$ s for the natural-ventilation case and at $t = 100$ s for the forced-ventilation cases. This approach ensures that the subsequent hydrogen dispersion is governed by a developed ventilation pattern rather than by initial transients. The total durations for natural and forced ventilation cases are 5,000 s and 800 s, respectively.

Table 2. Description of the simulated case studies.

Case	Ventilation	Charging mode	H_2 release	H_2 release rate (kg/s)	ACH (h^{-1})
1	Natural	Float	Since 200 s	1.31×10^{-5}	1
2	Forced	Boost	Since 100 s	3.42×10^{-5}	19
3	Forced	Exceptional	Since 100 s	1.05×10^{-3}	19

Using the same numerical setup and boundary conditions described in Section 2.1.2, eleven monitoring points were defined to analyze the hydrogen dispersion behavior. As shown in Figure 2, two monitors are located at the ventilation outlets (MP1, MP2), four at the room center at different elevations (MP3–MP6), four at the roof corners (MP7–MP10), and one at the opening on wall *Y1* (MP11). This allows for the consistent assessment of both the overall ventilation effectiveness and potential local hydrogen accumulation near the ceiling across all cases.

3. Results and Discussion

To provide a reference for the numerical results, the nominal steady-state hydrogen concentration was first estimated using a well-mixed control-volume approximation according to Equation C.1 from International Electrotechnical Commission (2022). Assuming a constant hydrogen release rate $\dot{m}_{\mathrm{H_2}}$ and a fixed ventilation exhaust rate $\dot{m}_{\mathrm{vent}}$, given the density of hydrogen and air at room temperature, the volumetric flow rate of hydrogen and ventilation can be calculated as $\mathrm{Q_{H_2}}$ and $\mathrm{Q_{vent}}$, respectively. The steady-state background concentration X_b can be approximated as

$$X_b = \frac{f \times \mathrm{Q_{H_2}}}{\mathrm{Q_{H_2}} + \mathrm{Q_{vent}}}. \qquad (1)$$

Where f is a mixing factor representing ventilation mixing efficiency; $f = 1$ is used in this study (ideal well-mixed assumption), whereas $f > 1$ indicates less efficient mixing, i.e., internal concentration gradients such that the outlet concentration is lower than the volume-average. The nominal hydrogen volume fractions for the three operating conditions are calculated to be 0.14 vol% for Case 1, 0.02 vol% for Case 2, and 0.59 vol% for Case 3, respectively. These values serve as theoretical benchmarks for comparison with the CFD-predicted transient and spatially resolved hydrogen concentrations. In this context, concentrations below 50% of the LFL are typically considered adequate to avoid area classification, whereas a threshold of 25% of the LFL (i.e., 1 vol%) is commonly used in standards and good practice as a conservative safety margin. Therefore, a hydrogen volume fraction of 1 vol% is adopted in this study as a reference level.

MP2, MP6, and MP7 were selected as representative monitoring points at the outlet, near the ceiling, and in a roof-corner region, respectively, to capture ventilation efficiency, vertical stratification, and possible local accumulation. Figure 4a shows the time evolution of hydrogen concentration for Case 1 – float charging under natural ventilation. After hydrogen release begins at $t = 200$ s, the concentration increases gradually at all three locations, reflecting the low release rate of float charging. Higher hydrogen volume fractions are consistently observed at MP6 and MP7, while MP2 remains lower throughout the simulation. By the end of the simulation, the hydrogen volume fraction near the ceiling reaches approximately 0.17–0.18 vol%, whereas the outlet concentration stabilizes at around 0.12 vol%. This vertical concentration gradient indicates buoyancy-driven accumulation in the upper part of the room. Compared with the forced-ventilation cases, natural ventilation leads to slower hydrogen removal and more pronounced stratification, although no abrupt fluctuations or localized peaks are observed.

Figure 4b shows the temporal evolution of hydrogen concentration for Case 2, corresponding to boost charging under forced ventilation. Following the onset of hydrogen release at $t = 100$ s, the hydrogen volume fraction increases steadily at all monitoring points and converges toward a quasi-steady state. Slightly higher concentrations are still observed near the ceiling, reaching approximately 0.03 vol% by the end of the simulation, while the ventilation outlet maintains a lower and more stable level around 0.02 vol%. This behavior indicates that, despite the presence of forced ventilation, some degree of hydrogen accumulation near the ceiling and vertical stratification persists under boost charging conditions, although the resulting concentration levels are markedly lower than in Case 1.

During the whole process, the maximum hydrogen concentration is located near the release areas, which stabilizes in the range of approximately 0.50–0.55 vol%. This value remains well below commonly used safety thresholds such as 25% of the LFL. No persistent localized hydrogen pockets are observed, and spatial gradients remain moderate throughout the room. These results demonstrate that, under boost charging conditions, forced ventilation is effective in limiting hydrogen accumulation and maintaining a low overall hazard level.

Under exceptional charging with forced ventilation, the hydrogen volume fraction shows clear transient behaviors (Figure 4c). After the start of hydrogen release, the hydrogen volume fraction increases rapidly at all monitoring locations. At the ventilation outlet (MP2) and the upper room center (MP6), the concentration rise is relatively smooth, and both locations gradually approach stable values in the range of approximately 0.8–1.0 vol%. In contrast, the monitor located near the roof-corner (MP7) exhibits pronounced unsteady behavior, three transient peaks can be witnessed that the hydrogen volume fraction temporarily increases to about 1.5–1.6 vol%, which is above the 25% LFL (1 vol%), but still within the range of 50% LFL (2 vol%). This indicates that at high release rates, high-concentration hydrogen pockets can still form even with strong forced ventilation, driven by the combined effects of buoyancy, room geometry, and local recirculation. Mitigation measures such as local extraction can be applied in this case.

Figure 5 shows the evolution of hydrogen concentration on a vertical *YZ* plane at $x = 6.78$ m, corresponding to the cross-section through one of the ventilation outlets. Under exceptional charging, hydrogen accumulates progressively beneath the ceiling as the buoyant plume spreads laterally, resulting in a gradual increase of concentration in the upper part of the room. In addition, the interaction between ventilation-induced flow and room geometry leads to localized accumulation near the lower part of wall *Y0*, where recirculation

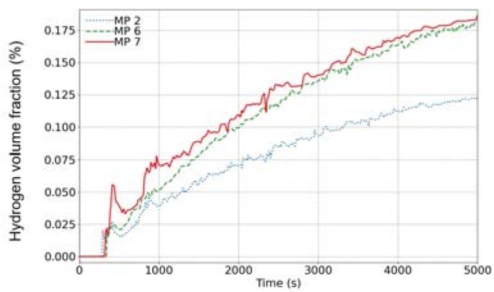

(a) Case 1

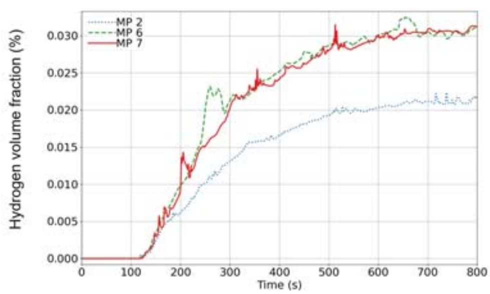

(b) Case 2

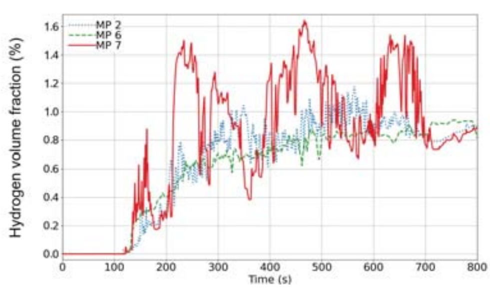

(c) Case 3

Fig. 4. Time evolution of hydrogen volume fraction (vol%) under three different conditions: (a) Case 1, (b) Case 2, and (c) Case 3.

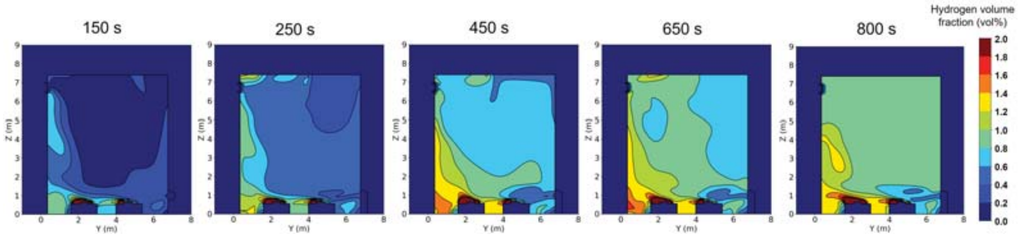

Fig. 5. Hydrogen accumulation and vertical stratification on a *YZ* plane at the ventilation outlet under exceptional charging (Case 3).

zones develop.

The peak values of leak surface hydrogen volume fraction at $t = 800$ s are observed to be up to 12.17 vol% locally and transiently, close to the release areas over the battery cells, indicating significant local enrichment. Figure 6 further illustrates the concentration distribution close to the leakage region. At $t = 800$ s, hydrogen concentrations exceeding the lower flammability limit extend to approximately 0.2 m above the leak, while concentrations above 50% LFL persist up to about 0.5 m. These results demonstrate that, even with strong forced ventilation, localized hazardous hydrogen pockets can form near the release region under exceptional charging conditions.

For Case 1 and Case 2, hydrogen concentrations measured near the ceiling remain higher than those at the ventilation outlets, indicating buoyancy-driven stratification even under forced ventilation in Case 2 due to the relatively low release rate. In Case 3, the much higher hydrogen release rate enhances mixing and flow unsteadiness, so the difference between ceiling and outlet concentrations becomes less clear toward the end of the simulation, even though local high concentrations still appear.

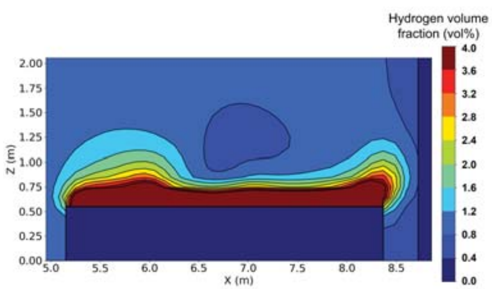

Fig. 6. Hydrogen concentration distribution on a *XZ* plane near the leakage region at $t = 800$ s for Case 3.

It is worth noting that simplified calculations (Eq. 1) are broadly consistent with the CFD predictions in terms of overall concentration level. For Case 1, the simplified calculation predicts a hydrogen concentration of 0.14 vol% that lies between the values measured near the ceiling (0.175 vol%) and those at the ventilation outlet (0.125 vol%). For Case 2, the hydrogen concentration at the ventilation outlet stabilizes around 0.02 vol%, matching the simplified estimate; the 25% LFL is never reached during the entire simulation, thus declassification of ATEX zones may be valid in this case. For Case 3, the final concentrations at the ventilation outlet and in the room center (around 0.9 vol%) are much higher than the calculated value (0.59 vol%), and the CFD simulations reveal the formation of localized high-concentration pockets near the ceiling and leakage regions (Figure 5). This demonstrates that, although simplified methods provide a reasonable estimate of average conditions, they may underestimate localized risks and flammable gas concentration under exceptional releases, underscoring the importance of CFD for assessing spatial non-uniformity and transient hydrogen accumulation in battery rooms.

4. Conclusion

This study employed CFD simulations using FLACS to investigate hydrogen dispersion in a full-scale Ni–Cd battery room under different charging and ventilation conditions, with particular attention to the limitations of simplified ventilation-based safety assessments. The results show that hydrogen concentrations predicted by CFD, especially at locations near the ceiling, are generally higher than those estimated using a well-mixed theoretical model, demonstrating that uniform-mixing assumptions can underestimate local and transient accumulation.

For natural ventilation with float charging and forced ventilation with boost charging (Cases 1 and 2), both CFD results and theoretical estimates indicate hydrogen levels well below 25% of the LFL, suggesting that these operating conditions can be considered safe within the studied configuration. In contrast, forced ventilation under exceptional charging (Case 3) leads to pronounced local and transient hydrogen accumulation, with CFD-predicted concentrations exceeding 25% LFL in localized regions, despite a relatively high overall air-change rate.

These findings indicate that, under high hydrogen release rates, compliance with standard ventilation criteria alone may not be sufficient to prevent the formation of hazardous hydrogen pockets. Additional mitigation measures, such as localized exhaust near leakage sources or ceiling regions and enhanced ventilation distribution, should be considered to ensure that the space remains unclassified under ATEX requirements. Overall, the study highlights the critical role of CFD in supporting risk-informed ventilation design and ATEX area classification for stationary battery installations.

Acknowledgement

The first author works within the framework of Project 101119358, 'PROSAFE', funded by the Marie Skłodowska-Curie Actions programme, HORIZON-MSCA-2022-DN-01. This work was also partly funded by Grant PID2023-150607OB-I00 funded by MICIU/AEI/ 10.13039/501100011033 and by ERDF/EU.

References

American Society of Mechanical Engineers (ASME) (2008, July). Procedure for estimation and reporting of uncertainty due to discretization in cfd applications. *Journal of Fluids Engineering 130*(7), 078001.

Brzezińska, D. (2018). Ventilation system influence on hydrogen explosion hazards in industrial lead-acid battery rooms. *Energies 11*(8), 2086.

ElNakeeb, M. A., A. E. El-Degwy, and E. E. Khalil (2017). Effect double vertical batteries storage on hydrogen concentration in air conditioned storage room. *Procedia Engineering 205*, 4172–4178.

European Parliament and the Council (2014). Directive 2014/34/eu of the european parliament and of the council on the harmonisation of the laws of the member states relating to equipment and protective systems intended for use in potentially explosive atmospheres. *Official Journal of the European Union*.

Gexcon AS (2025, January). *FLACS-CFD v24.2 User's Manual*. Copyright © Gexcon AS, January 15, 2025.

International Electrotechnical Commission (2010). Safety requirements for secondary batteries and battery installations – part 2: Stationary batteries. IEC Standard 62485-2.

International Electrotechnical Commission (2022). Explosive atmospheres - part 10-1: Classification of areas - explosive gas atmospheres. IEC Standard 60079-10-1.

Lu, T. and J. Gong (2021). Affecting mechanism of partition boards on hydrogen dispersion in confined space with symmetrical lateral openings. *International Journal of Hydrogen Energy 46*(78), 38944–38958.

Nan, F., Z. Luo, F. Cheng, Y. Xiao, R. Li, B. Su, and T. Wang (2024). Research progress and development trends of hydrogen explosion suppression materials and mechanisms. *Process Safety and Environmental Protection 184*, 1318–1331.

Roache, P. J. (1997). Quantification of uncertainty in computational fluid dynamics. *Annual Review of Fluid Mechanics 29*(1), 123–160.